Supplement of

Three-dimensional atmospheric circulation teleconnections in the Northern Hemisphere

Haihong Yang[1], Shujuan Hu[1,2], Jianjun Peng[3] Wenxin Zhang[1], Zihan Hao[1], Yuchen Wu[1], and Zhiwei Zhu[4]

[1] College of Atmospheric Sciences, Lanzhou University, Lanzhou730000, China

[2] Collaborative Innovation Center for Western Ecological Safety, Lanzhou University, Lanzhou, China

[3] State Key Laboratory of Tropical Oceanography, South China Sea Institute of Oceanology, Chinese Academy of Sciences, Guangzhou, China

[4] State Key Laboratory of Climate System Prediction and Risk Management/Key Laboratory of Meteorological Disaster, Ministry of Education/Collaborative Innovation Center on Forecast and Evaluation of Meteorological Disasters, Nanjing University of Information Science and Technology, Nanjing 210044, China

Methods

Three-pattern decomposition of global atmospheric circulation (3P-DGAC)

To achieve a more objective and realistic representation of atmospheric circulation, Hu et al. (2017, 2018a, b, 2020) developed a novel method called the three-pattern decomposition of global atmospheric circulation (3P-DGAC), which dynamically treats the actual atmosphere as an integrated system. In contrast to traditional two-dimensional (2D) decomposition techniques that neglect vertical motion in mid- to high-latitudes and horizontal vortex dynamics in low latitudes, 3P-DGAC accounts for these processes, enabling a more complete diagnosis of real atmospheric dynamics. Specifically, this method generalizes mid-latitude Rossby wave activity as well as Hadley and Walker circulations in the tropics to a global framework. It conceptualizes atmospheric circulation as a superposition of three components: horizontal vortex, meridional, and zonal circulations. Furthermore, 3P-DGAC quantitatively separates the three-dimensional (3D) vertical vorticity into horizontal rotational and divergent parts, thereby improving the consistency with observed atmospheric behavior. It defines three stream functions corresponding to three orthogonal planes—horizontal circulation in the horizontal plane, meridional circulation in the meridional vertical plane, and zonal circulation in the zonal vertical plane. **For clarity, we adopt the notations ψ_σ, ψ_λ, and ψ_φ to replace the original R, H, and W stream functions(Hu et al. 2017, 2018a, b).** This decomposition technique has been increasingly applied in studies of abnormal weather and climate events to construct physically meaningful mechanism frameworks (Peng et al. 2023, 2024; Zhou et al. 2023; Hu et al. 2025). In this study, we present only a brief summary of the key steps involved in 3P-DGAC for simplicity.

To resolve the unit inconsistency associated with 3D vorticity calculations in the pressure (p) coordinate system, the 3P-DGAC adopts a spherical sigma (σ) coordinate framework. For broader applicability, the transformation from σ-coordinates to p-coordinates is approximated as follows:

$$u' = \frac{u}{a},\ v' = \frac{v}{a},\ \ \dot{\sigma} = \frac{\omega}{P_S},\ \sigma = \frac{p}{P_S}, \tag{1}$$

where a is the radius of the earth, p is the pressure, and P_S = 1000 hPa is the sea level pressure. (u, v, ω) and $(u', v', \dot{\sigma})$ denote the three velocity components in the spherical p-coordinate system and spherical σ-coordinate system, respectively. Typically, we employ formula (1) to convert variables from σ-coordinate to p-coordinate.

According to the theory of the 3P-DGAC, the stream functions ψ_σ, ψ_λ, and ψ_φ are defined in the spherical σ-coordinate system as follows:

$$\begin{cases} \Delta_3\psi_\sigma = \Delta_2\psi_\sigma + \dfrac{\partial^2\psi_\sigma}{\partial\sigma^2} = \zeta, \\ \psi_\lambda = \displaystyle\int_0^\sigma (\frac{1}{\sin\theta}\frac{\partial\psi_\sigma}{\partial\lambda} - v')d\sigma = \int_0^\sigma (v'_\sigma - v')d\sigma = -\int_0^\sigma v'_\lambda d\sigma, \\ \psi_\varphi = \displaystyle\int_0^\sigma (\frac{\partial\psi_\sigma}{\partial\theta} + u')d\sigma = \int_0^\sigma (u' - u'_\sigma)d\sigma = \int_0^\sigma u'_\varphi d\sigma. \end{cases} \tag{2}$$

Then, the components of atmospheric circulation in the 3P-DGAC model can be expressed as

$$\begin{cases} u' = u'_\varphi + u'_\sigma = \dfrac{\partial\psi_\varphi}{\partial\sigma} - \dfrac{\partial\psi_\sigma}{\partial\theta}, \\ v' = v'_\sigma + v'_\lambda = \dfrac{1}{\sin\theta}\dfrac{\partial\psi_\sigma}{\partial\lambda} - \dfrac{\partial\psi_\lambda}{\partial\sigma}, \\ \dot\sigma = \dot\sigma_\lambda + \dot\sigma_\varphi = \dfrac{1}{\sin\theta}\dfrac{\partial(\sin\theta\psi_\lambda)}{\partial\theta} - \dfrac{1}{\sin\theta}\dfrac{\partial\psi_\varphi}{\partial\lambda}. \end{cases} \tag{3}$$

Where $\zeta = \dfrac{1}{\sin\theta}\dfrac{\partial v'}{\partial\lambda} - \dfrac{1}{\sin\theta}\dfrac{\partial(u'\sin\theta)}{\partial\theta} = \dfrac{1}{a\sin\theta}\dfrac{\partial v}{\partial\lambda} - \dfrac{1}{a\sin\theta}\dfrac{\partial(u\sin\theta)}{\partial\theta}$ represents the relative vorticity of the actual atmosphere, which consists of two components, one arises from the horizontal vortex motion and another is generated by the divergence of the large-scale vertical circulations, they are denoted by $\Delta_2\psi_\sigma = \dfrac{1}{\sin\theta}\dfrac{\partial v'_\sigma}{\partial\lambda} - \dfrac{1}{\sin\theta}\dfrac{\partial u'_\sigma}{\partial\theta}$ and $\dfrac{\partial^2\psi_\sigma}{\partial\sigma^2} = \dfrac{1}{\sin\theta}\dfrac{\partial v'_\lambda}{\partial\lambda} - \dfrac{1}{\sin\theta}\dfrac{\partial u'_\varphi\sin\theta}{\partial\theta}$. Here $\Delta_3 = \dfrac{1}{\sin^2\theta}\dfrac{\partial^2}{\partial\lambda^2} + \dfrac{1}{\sin\theta}\dfrac{\partial}{\partial\theta}(\sin\theta\dfrac{\partial}{\partial\theta}) + \dfrac{\partial^2}{\partial\sigma^2}$ and $\Delta_2 = \dfrac{1}{\sin^2\theta}\dfrac{\partial^2}{\partial\lambda^2} + \dfrac{1}{\sin\theta}\dfrac{\partial}{\partial\theta}(\sin\theta\dfrac{\partial}{\partial\theta})$ are behalf of the 3D and 2D Laplace operators, respectively, in the spherical σ-coordinate system; u' and v' are the horizontal velocities of the actual atmosphere in the spherical σ-coordinate; $\dot\sigma$ is the vertical velocity; (u'_σ, v'_σ), $(u'_\phi, \dot\sigma_\phi)$ and $(v'_\lambda, \dot\sigma_\lambda)$ are the velocities of the horizontal, zonal, and meridional circulations, respectively; θ is the colatitude and λ is the longitude.

It's worth noting that when $p = P_S$ (the sea level pressure), the velocity fields typically adhere to the following boundary conditions in the spherical p-coordinate system:

$$\omega = 0, \ \frac{\partial u}{\partial p} = 0, \ \frac{\partial v}{\partial p} = 0. \tag{4}$$

Thus, when σ=1 in the spherical σ-coordinate system, the boundary conditions are expressed as:

$$\dot{\sigma} = 0, \ \frac{\partial u'}{\partial \sigma} = 0, \ \frac{\partial v'}{\partial \sigma} = 0. \tag{5}$$

Based on the representing relationship between stream functions and the velocity fields (Eq. (3)), when $\sigma = 1$, the stream functions satisfy the following boundary conditions:

$$\psi_\lambda = \psi_\varphi = 0, \ \frac{\partial \psi_\sigma}{\partial \sigma} = 0. \tag{6}$$

Then, using the boundary conditions (6), we can solve the equations (2) to obtain the stream functions ψ_λ, ψ_φ, ψ_σ and the velocity fields of the three circulations, which leads to the 3P-DGAC. It should be noted in particular that in this study, all the decomposed velocities computed by the 3P-DGAC are converted to the expression in p-coordinate via formula (1). Additional details on the 3P-DGAC method can be found from Hu et al. (2017, 2018a, b).

Figures

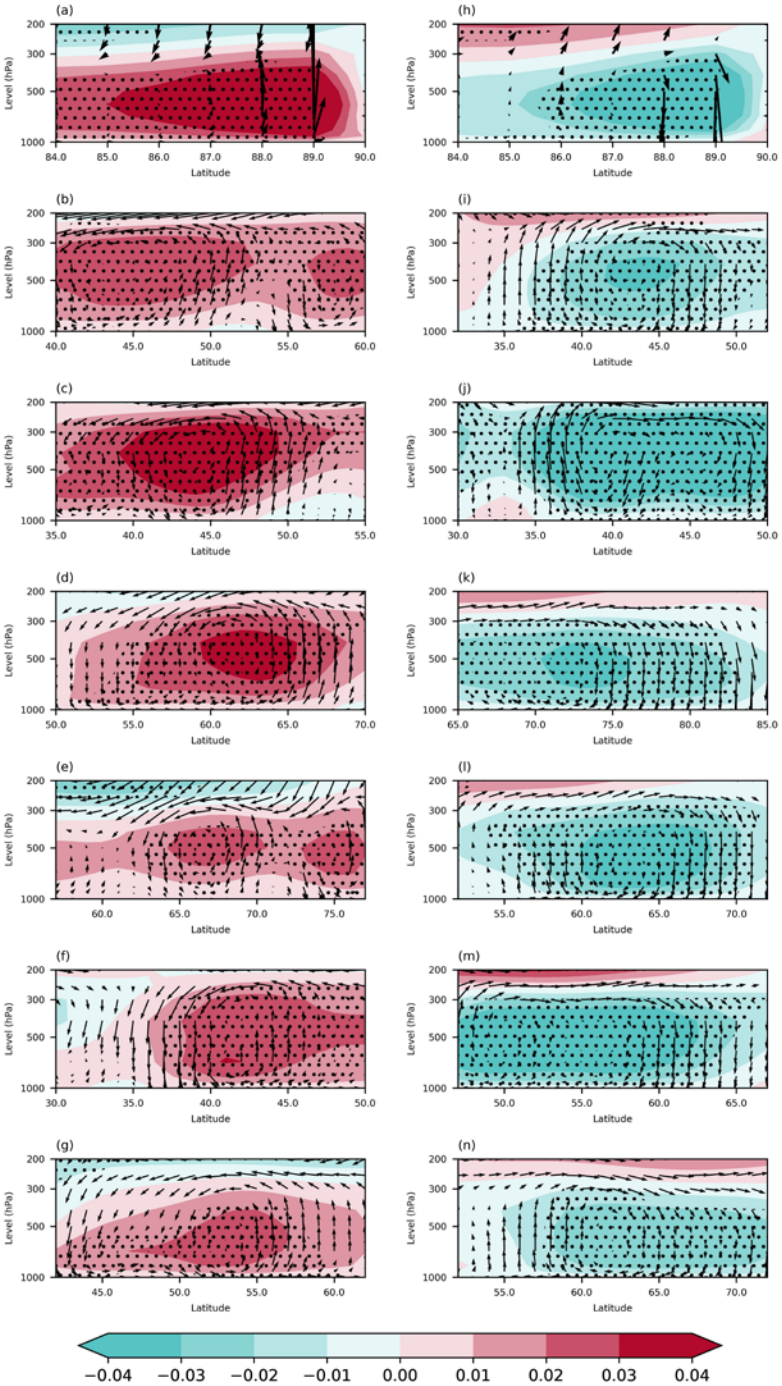

Figure S1. Meridional vertical circulation teleconnection patterns: a pair of counter-rotating local meridional vertical circulations. (a)((b)-(g))Regressions of stream function H(shading units:$10^{-6}m^{-1}$) of meridional circulation along the meridional cross-sections at the pole A of HP (HCB HCST, HSK, HGS, HBA, and HUB) onto HPI (HCBI, HCSTI, HSKI, HGSI, HBAI, and HUBI) during the summer for the period of 1979-2022. The data are detrended before analysis, and the areas significant at the 95% confidence level are dotted. (h)-(n) As in (a)-(g), but for the pole B of HP, HCB, HCST, HSK, HGS, HBA, and HUB.

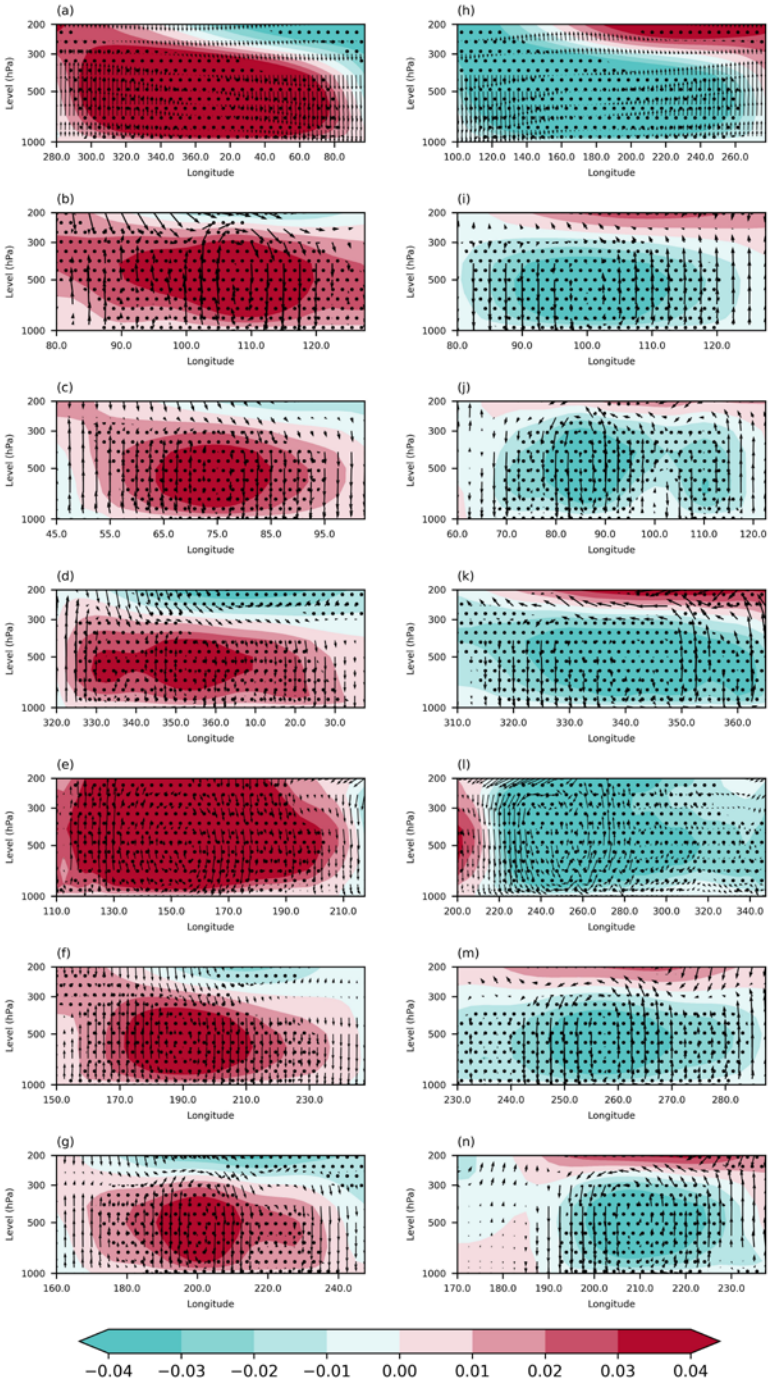

Figure S2. Zonal vertical circulation teleconnection patterns: a pair of counter-rotating local Zonal vertical circulations. (a)((b)–(g))Regressions of stream function W(shading units:$10^{-6}m^{-1}$) of zonal circulation along the zonal cross-sections at the pole A of WP (WMCS, WGA, WOM, WWSJ, WCV, and WBA) onto WPI (WMCSI, WGAI, WOMI, WWSJI, WCVI, and WBAI) during the summer for the period of 1979-2022. The data are detrended before analysis, and the areas significant at the 95% confidence level are dotted. (h)-(n) As in (a)-(g), but for the pole B of WP, WMCS, WGA, WOM, WWSJ, WCV, and WBAI

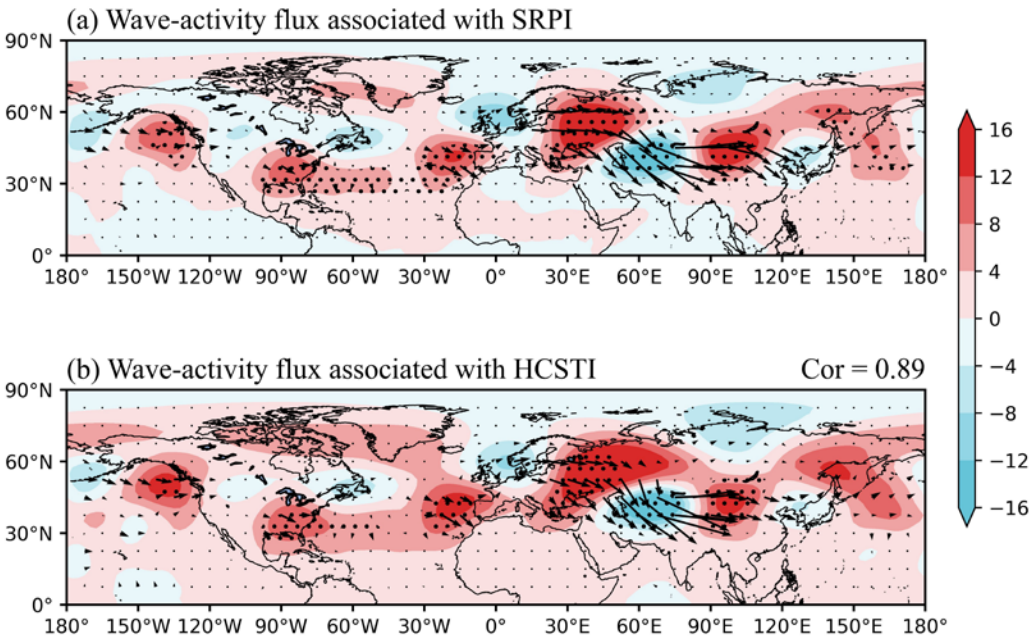

Figure S3. Wave-activity flux associated with SRPI and HCSTI. (a) Regressed summer 200-hPa GHT anomalies (shading, units: gpm) onto Silk-Road pattern index for the period of 1979-2022. The horizontal wave-activity fluxes associated with Silk-Road pattern (black arrow, units: 10^{-1} m^2 s^{-2}). (b) As in (a), but for Caspian Sea-Tarim pattern. The correlation coefficient during 1979-2022 between SRPI and HCSTI is also shown in the figure, which in bold represents it was significant at the 99% confidence level.

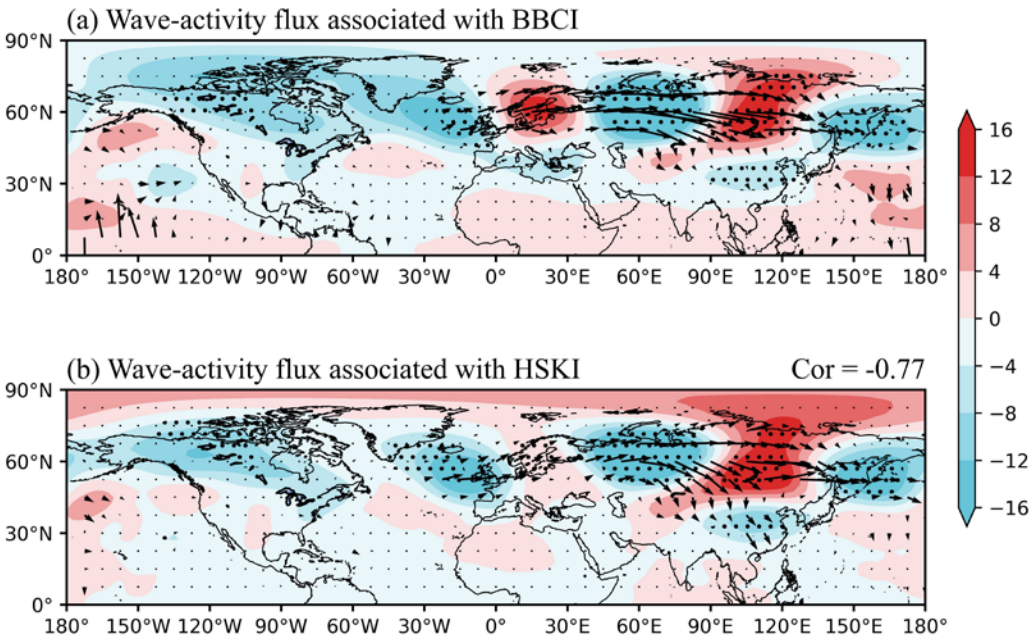

Figure S4. Wave-activity flux associated with BBCI and HSKI. (a) Regressed summer 200-hPa GHT anomalies (shading, units: gpm) onto the British–Baikal Corridor Pattern index (BBCI) for the period of 1979-2022. The horizontal wave-activity fluxes associated with the British–Baikal Corridor Pattern are shown (black arrows, units: 10^{-1} m^2 s^{-2}). (b) As in (a), but for the Central Siberian Plateau–Kara Sea Pattern. For ease of comparison, (b) shows the regression of the negative HSKI. The correlation coefficient between BBCI and HSKI during 1979–2022 is also shown in the figure, with bold values indicating significance at the 99% confidence level.

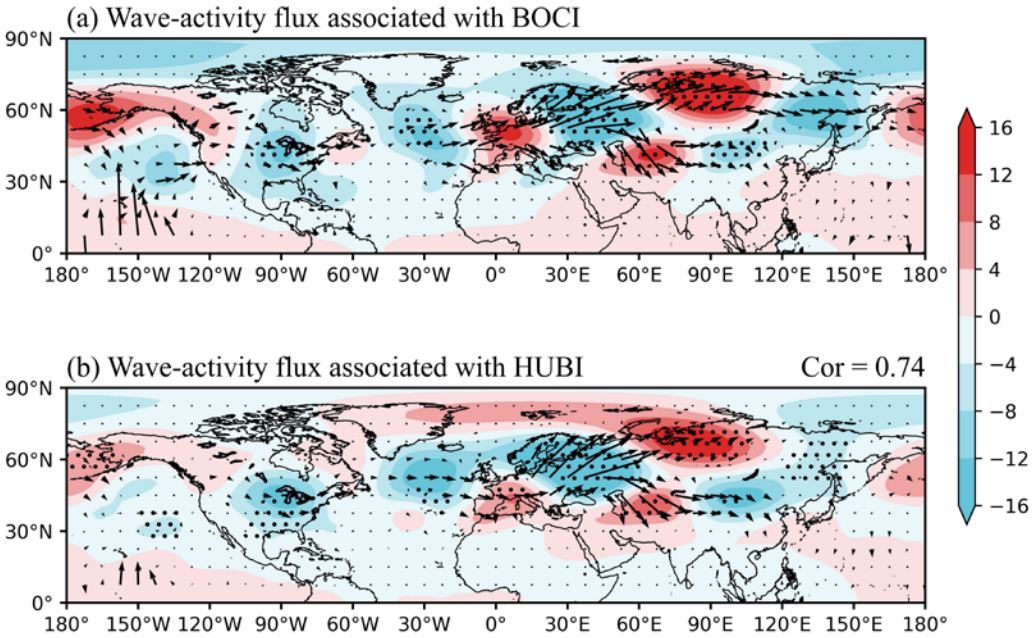

Figure S1. Wave-activity flux associated with BOCI and HUBI. (a) Regressed summer 200-hPa GHT anomalies (shading, units: gpm) onto BOCI for the period of 1979-2022. The horizontal wave-activity fluxes associated with British-Okhotsk Corridor pattern (black arrow, units: 10^{-1} m^2 s^{-2}). (b) As in (a), but for Baltic sea - Ural-Baltic pattern (HUB). the correlation coefficient during 1979-2022 between BOCI and HUBI is also shown in the figure, which in bold represents it was significant at the 99% confidence level.

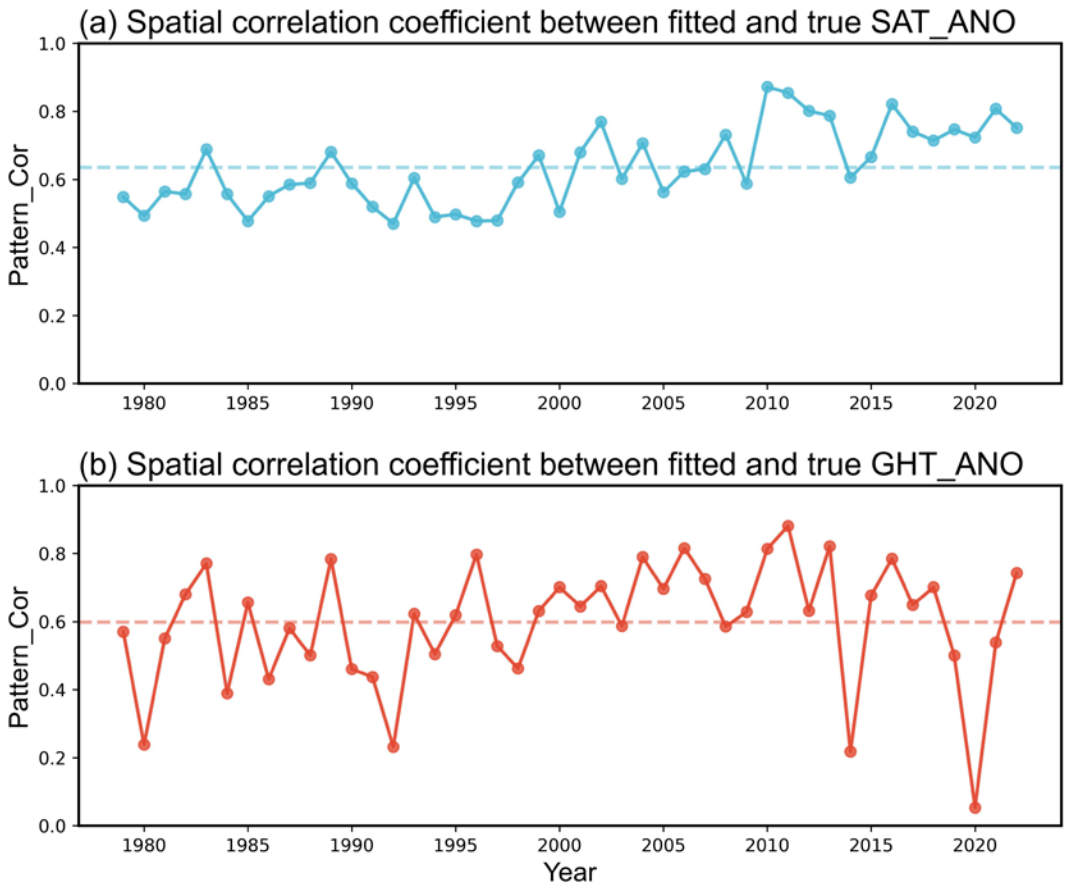

Figure S6.Interannual Reconstruction Skill of Summer Climate Variability. (a) Time series of spatial correlation coefficients between reconstructed and observed surface temperature anomalies for Northern Hemisphere summers (1979–2022). (b) As in (a), but for geopotential height anomalies. Dashed lines represent the multi-decadal average values.

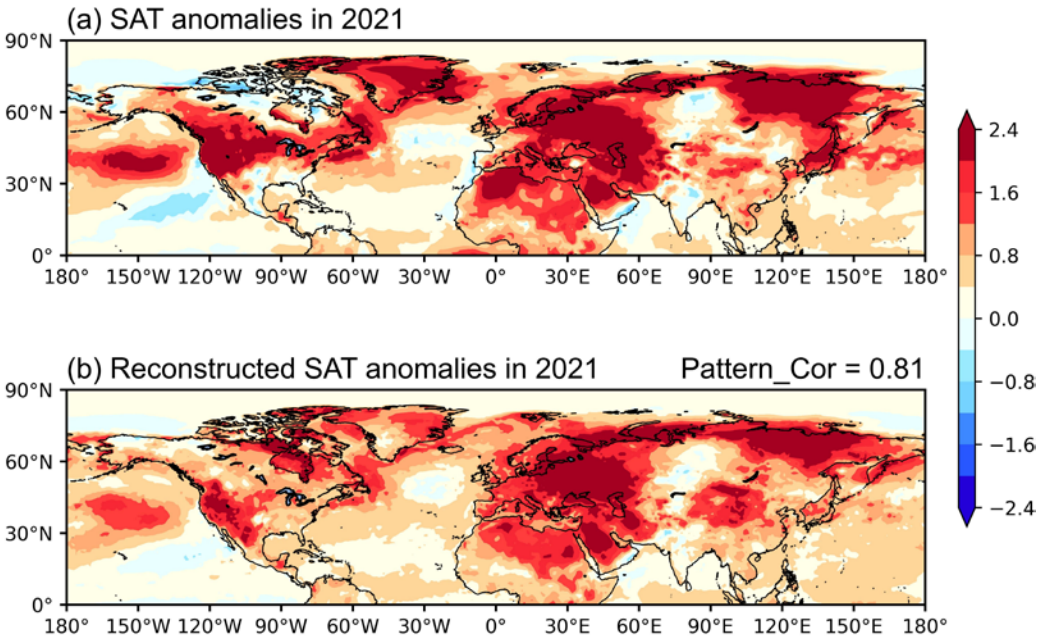

Figure S7. Combined effect of global warming and atmospheric circulation pattern on summer SAT of 2021. (a) SAT anomalies (shading, units: °C) in the NH during the summers of 2021. (b) Reconstructed summer SAT anomalies (shading, units: °C) in the NH during the summers of 2021.

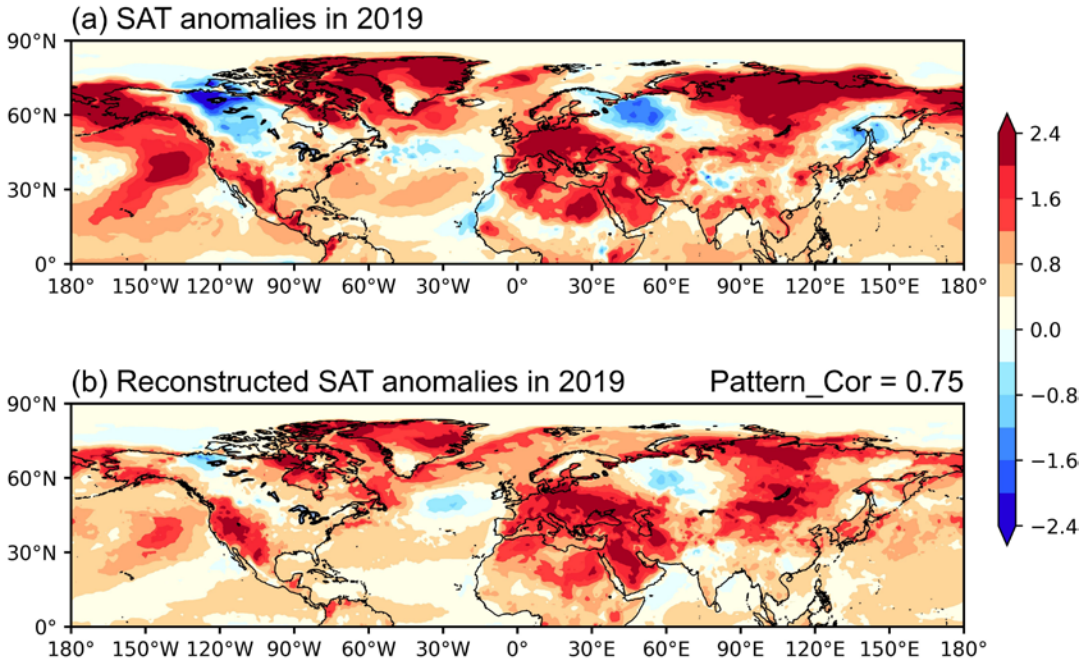

Figure S8. Combined effect of global warming and atmospheric circulation pattern on summer SAT of 2019. (a) SAT anomalies (shading, units: °C) in the NH during the summers of 2019. (b) Reconstructed summer SAT anomalies (shading, units: °C) in the NH during the summers of 2019.

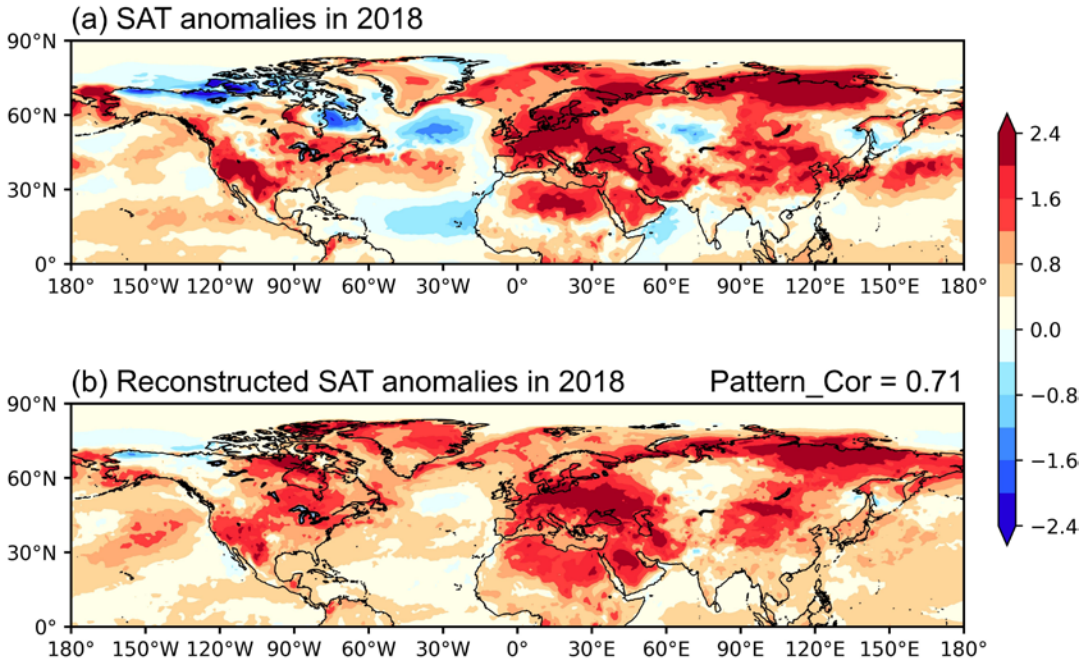

Figure S9. Combined effect of global warming and atmospheric circulation pattern on summer SAT of 2018. (a) SAT anomalies (shading, units: °C) in the NH during the summers of 2018. (b) Reconstructed summer SAT anomalies (shading, units: °C) in the NH during the summers of 2018.

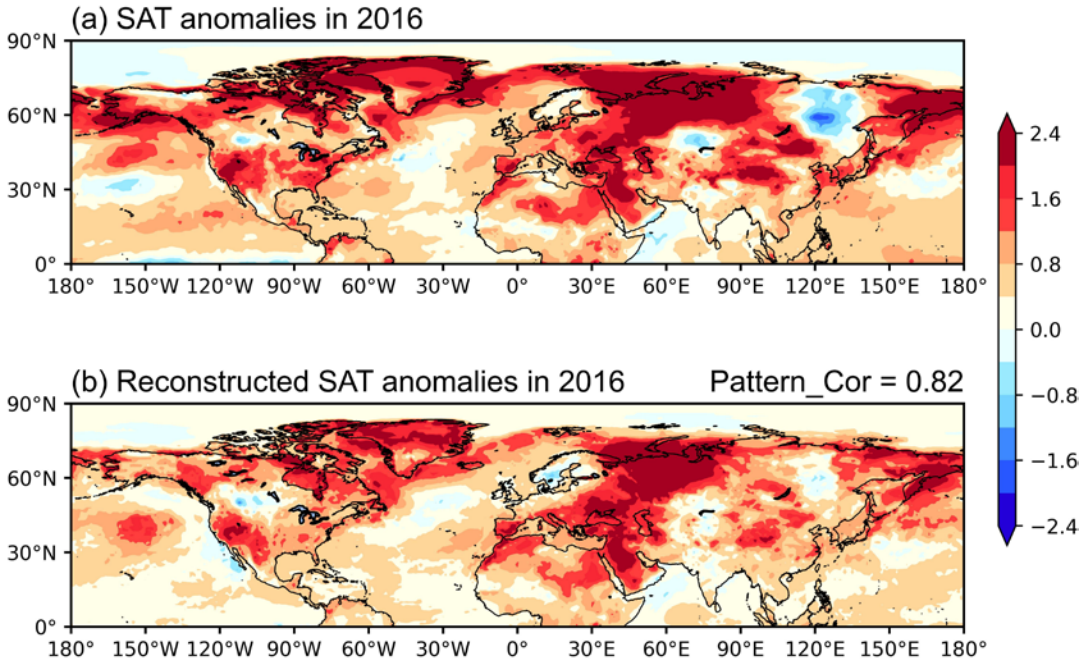

Figure S10. Combined effect of global warming and atmospheric circulation pattern on summer SAT of 2016. (a) SAT anomalies (shading, units: °C) in the NH during the summers of 2016. (b) Reconstructed summer SAT anomalies (shading, units: °C) in the NH during the summers of 2016.

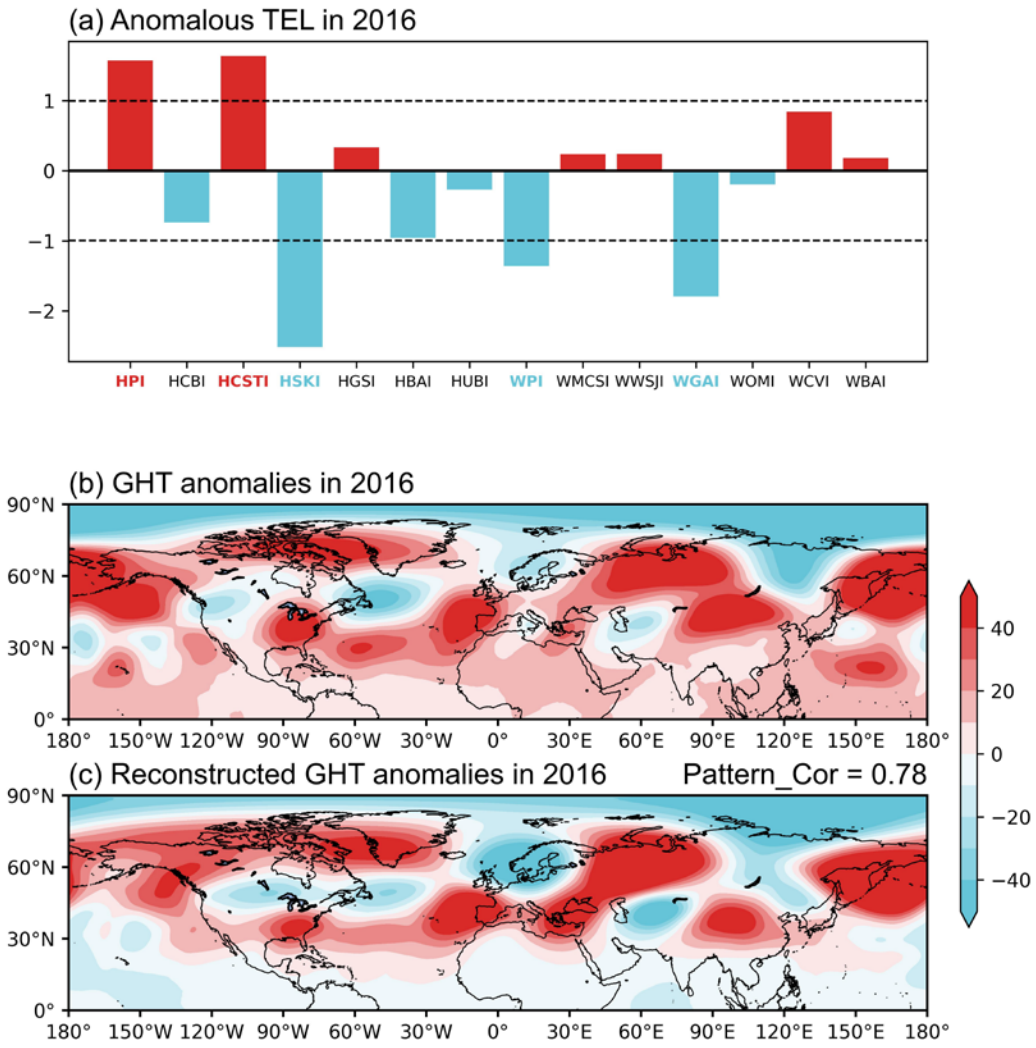

Figure S11. Reconstructed circulation anomalies in 2016. (a) Indices of teleconnection patterns in 2016. The dashed lines denote the reference line of the 1 standard deviation. (b) Summer GHT anomalies (shading, units: gpm) in the NH during the summer of 2016. (c) Reconstructed Summer GHT anomalies (shading, units: gpm) in the NH during the summers of 2016.

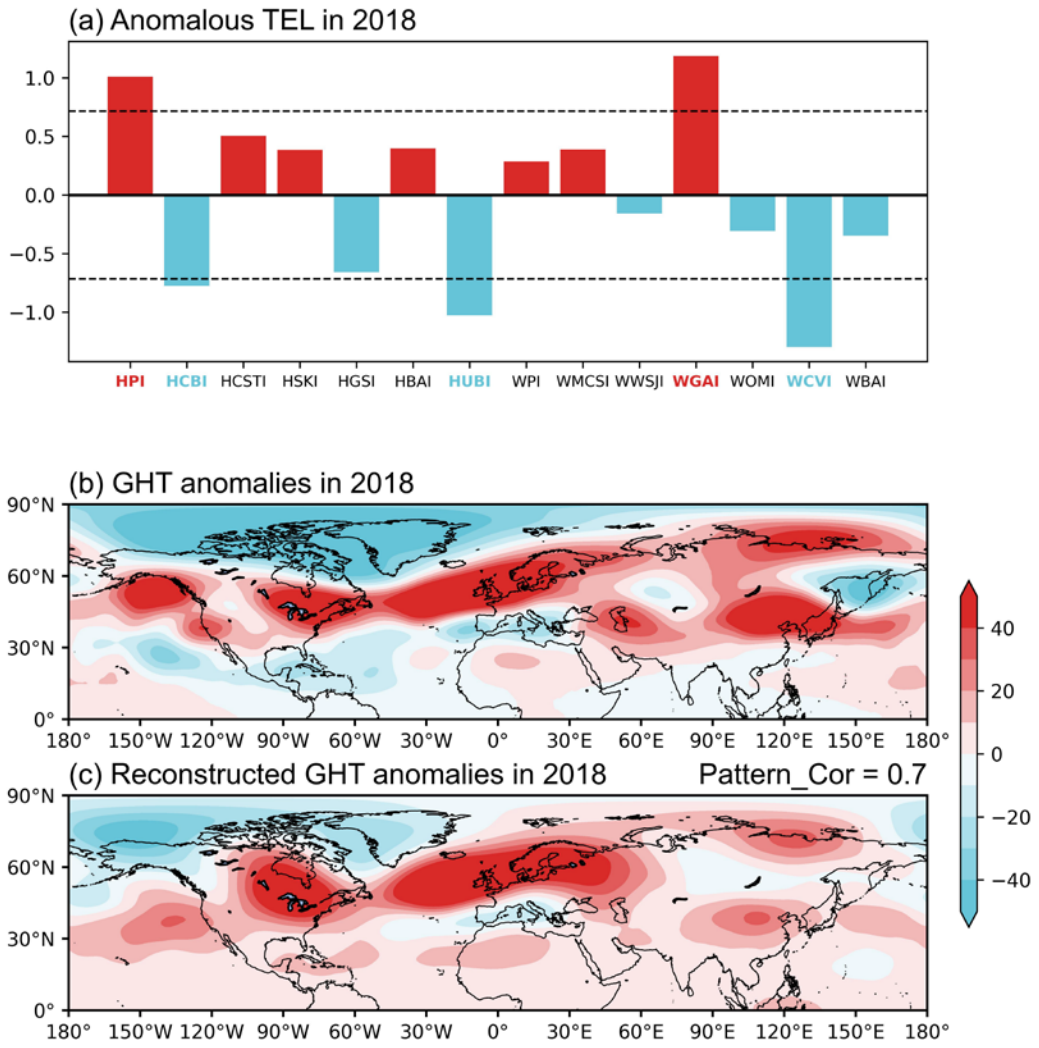

Figure S12. Reconstructed circulation anomalies in 2018. (a) Indices of teleconnection patterns in 2018. The dashed lines denote the reference line of the 1 standard deviation. (b) Summer GHT anomalies (shading, units: gpm) in the NH during the summer of 2018. (c) Reconstructed Summer GHT anomalies (shading, units: gpm) in the NH during the summers of 2018.

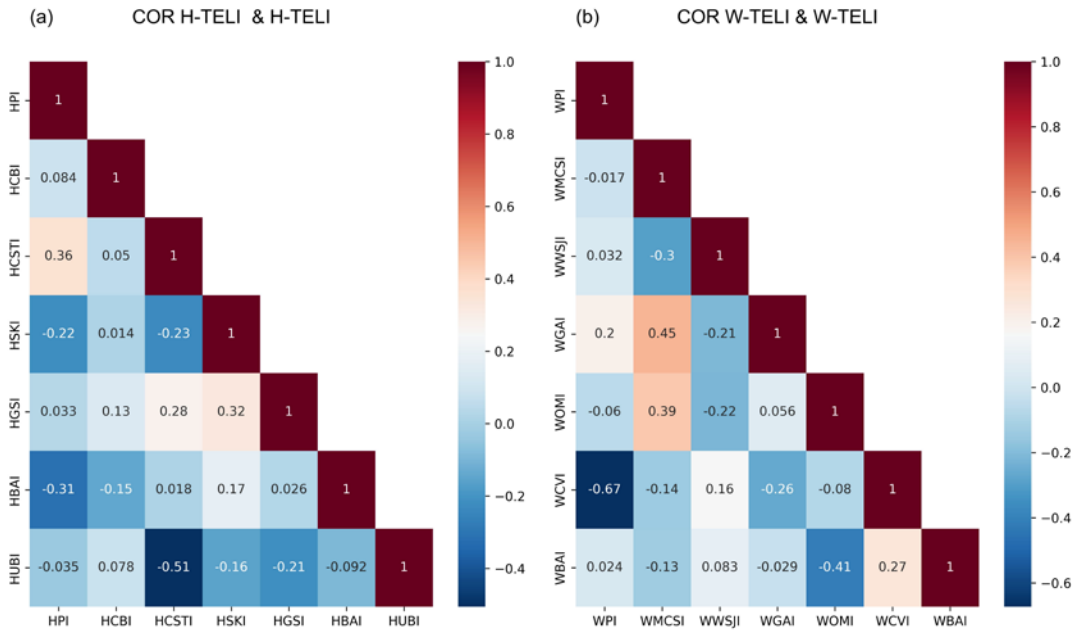

Figure S13. Correlation heatmap of seven teleconnection indices. (a: HPI, HCBI, HCSTI, HSKI, HGSI, HBAI, and HUBI. b: WPI, WMCSI, WGAI, WOMI, WWSJI, WCVI, and WBAI).

Tables

Table S1. Definition of the atmospheric circulation pattern indices. HPI (HCBI, HCSTI, HSKI, HGSI, HBAI, and HUBI) is abbreviation for Polar I pattern index (Canadian-Bermuda pattern index, Caspian-Tarim pattern index, Kara Sea-West Siberian pattern index, Greenland-Scandinavia pattern index, Black Sea-Aleutian pattern index, and Baltic-Ural pattern index and Baltic sea- Ural mountain pattern index. The second and third columns show the regions (Pole A and Pole B) used to define the atmospheric circulation pattern indices. The final column shows correlation coefficients between the two poles of the atmospheric circulation patterns, and the bold indicates significant at the 99.99% confidence level based on the Student's t-test.

H-TEL	Pole A		Pole B		Cor(Pole A, Pole B)*
HP	North Pole	(87.5, 87.5)	North Pole	(265, 87.5)	**-0.89**
HCB	Canadian Plains	(260, 50)	Bermuda Island	(292.5, 42.5)	**-0.76**
HCST	Caspian Sea	(50, 45)	Tarim Basin	(82.5, 40)	**-0.73**
HSK	Central Siberian Plateau	(127.5, 60)	Kara Sea	(75, 80)	**-0.71**
HGS	Greenland island	(320, 67.5)	Scandinavian peninsula	(7.5, 62.5)	**-0.68**
HBA	Black Sea	(30, 40)	Aleutian islands	(197.5, 57.5)	**-0.68**
HUB	Baltic sea	(17.5, 52.5)	Ural mountain	(57.5, 62.5)	**-0.67**

Table S2. Definition of the atmospheric circulation pattern indices. WPI (WMCSI, WGAI, WOMI, WWSJI, WCVI, and WBAI) is abbreviation for Pole II pattern index (Mongolia-Central Siberia pattern index, Greenland Sea-Azores pattern index, Ogasawara-Mexico pattern index, West Siberian-Junggar pattern index, Chukchi Sea-Victoria pattern index, and Bering Strait-Aleutian pattern index. The second and third columns show the regions (Pole A and Pole B) used to define the atmospheric circulation pattern indices. The final column shows correlation coefficients between the two poles of the atmospheric circulation patterns, and the bold indicates significant at the 99.99% confidence level based on the Student's t-test.

W-TEL	Pole A		Pole B		Cor(Pole A, Pole B)*
WP	North Pole	(347.5, 87.5)	North Pole	(167.5, 87.5)	**-0.90**
WMCS	Mongolian plateau	(107.5, 42.5)	Central Siberia Plain	(100, 67.5)	**-0.77**
WGA	Greenland sea	(355, 70)	Azores islands	(340, 45)	**-0.74**
WOM	Ogasawara Islands	(155, 25)	Gulf of Mexico	(75, 80)	**-0.76**
WWSJ	West Siberia plain	(77.5, 65)	Junggar Basin	(7.5, 62.5)	**-0.75**
WCV	Chukchi Sea	(187.5, 80)	Victoria island	(197.5, 57.5)	**-0.72**
WBA	Bering Strait	(197.5, 70)	Aleutian islands	(57.5, 62.5)	**-0.70**